THE JOURNAL OF PHYSICAL CHEMISTRY B

Article

pubs.acs.org/JPCB

UV Resonance Raman and DFT Studies of Arginine Side Chains in Peptides: Insights into Arginine Hydration

Zhenmin Hong, Jonathan Wert, and Sanford A. Asher*

Department of Chemistry, University of Pittsburgh, Pennsylvania 15260, United States

ABSTRACT: We examined the UV resonance Raman (UVRR) spectra of four models of the Arg side chain, guanidinium (Gdn), ethylguanidinium (EG), arginine (Arg), and Ac-Arg-OMe (AAO) in H_2O and D_2O, in order to identify spectral markers that report on the environment of the Arg side chain. To elucidate the resonance Raman enhancement mechanism of the Arg side chain, we used density functional theory (DFT) to calculate the equilibrium geometries of the electronic ground state and the first excited state. We determined the vibrational mode frequencies of the ground state and the first derivative of the first electronic excited state potential energy with respect to each vibrational normal mode of the electronic ground state at the electronic ground state equilibrium geometry. The DFT calculations and the potential energy distributions reveal that, in addition to the Gdn group C−N stretching vibrations, the C−N bond stretching vibration of the Gdn group-methylene linkage is also strongly resonance-enhanced in EG, Arg, and AAO. From the UVRR spectra, we find that the Raman cross section and frequency of the ∼1170 cm^{-1} vibration of the Arg side chain depends on its hydration state and can be used to determine the hydration state of the Arg side chain in peptides and proteins. We examined the hydration of the Arg side chain in two polyAla peptides and found that in the α-helical conformation the Arg side chain in the AEP peptide (sequence: $A_9RA_3EA_4RA_2$) is less hydrated than that in the AP peptide (sequence: $A_8RA_4RA_4RA_2$).

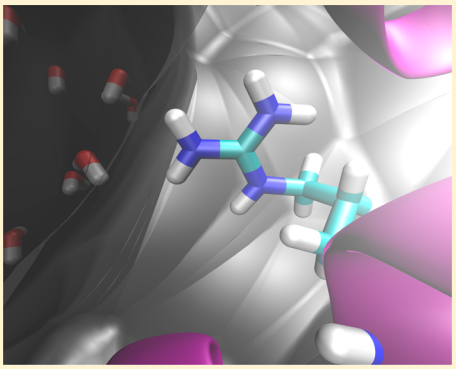

INTRODUCTION

UV resonance Raman (UVRR) spectroscopy has been shown to be a powerful tool to study the conformations and folding dynamics of peptides and proteins.[1−10] Excitation in the deep UV (<230 nm) selectively excites protein backbone vibrations and amino acid side chain vibrations. The side chain vibrations are sensitive to hydration and hydrogen bonding. The UVRR spectra of tryptophan,[11−18] tyrosine,[11−13,19] phenylalanine,[11,12,19] and histidine[18,20] have been extensively studied, while the UVRR spectrum of the arginine (Arg) side chain that is resonance enhanced by ∼200 nm excitation has been little investigated.

Hudson and co-workers[21] systematically studied the electronic and vibrational modes of guanidinium (Gdn) and some substituted derivatives. They studied the excitation profiles of Gdn, methylguanidinium, and *N*,*N*-dimethylguanidinium in both H_2O and D_2O. They calculated the electronic ground and first excited states of these compounds using the semiempirical intermediate neglect of differential overlap/screened approximation (INDO/S) method and assigned some of the Raman bands; however, due to their relatively poor spectral resolution and their poor signal-to-noise ratios, they were unable to study ethylguanidinium (EG) and Arg in detail.

The Arg side chain is positively charged up to pH 12 and should be strongly hydrated in water. Early measurements of the Arg amino acid distribution coefficient between water and the vapor phase suggested that Arg is the most hydrated residue; the hydration energy is double that of negatively charged Asp or Glu.[22] More recent studies implied that Arg might not be as hydrated as previously suggested. Mason et al.,[23−25] on the basis of neutron diffraction and molecular dynamics (MD) simulations, claimed that Gdn could form dimers in aqueous solution. Hunger et al.[26] used broadband dielectric relaxation spectroscopy to examine the hydration of Gdn and found that Gdn does not bind strongly to water molecules. McQuinn et al.[27] utilized energy-dependent ESI-MS/MS to study the dehydration of Gdn-water and methylated Gdn-water nanodroplets and found that the number of water molecules bound to the Gdn group decreases upon alkyl group substitution. These studies suggest that the Gdn group in Arg might not be very hydrated.

García et al.,[28] using MD simulations, calculated that the mean residence time of water in the hydration shells of Arg residues in proteins was comparable, and even slightly less than that of negatively charged Asp and Glu; this result indicated that Arg is not more hydrated than the other charged residues. The conclusions of García et al. were later confirmed by whole-residue hydrophobicity scales obtained by measuring the transfer free energy of a specific residue in a host peptide from water to a bilayer interface or to *n*-octanol.[29] On the whole-residue hydrophobicity scale, Arg is the least hydrated charged residue (among Lys, His, Glu, and Asp).

We here extend the work of Hudson and co-workers to EG, Arg, and *N*-acetyl arginine methyl ester (Ac-Arg-OMe, AAO). The ethyl substituent of EG breaks the Gdn symmetry, turning on some Raman inactive vibrations in Gdn to result in a different

Received: August 24, 2012
Revised: May 14, 2013
Published: May 15, 2013

   dx.doi.org/10.1021/jp404030u | *J. Phys. Chem. B* 2013, 117, 7145−7156

UVRR spectrum. AAO is an *N*-acetyl-capped arginine methyl ester, modeling the Arg residue in peptides. Our recent study on the Arg residue Raman excitation profile suggested that the Arg side chain electronic transitions would interact with the peptide backbone amide $\pi-\pi^*$ transition.[30] Figure 1 shows the molecular structures of Gdn, EG, Arg, and AAO.

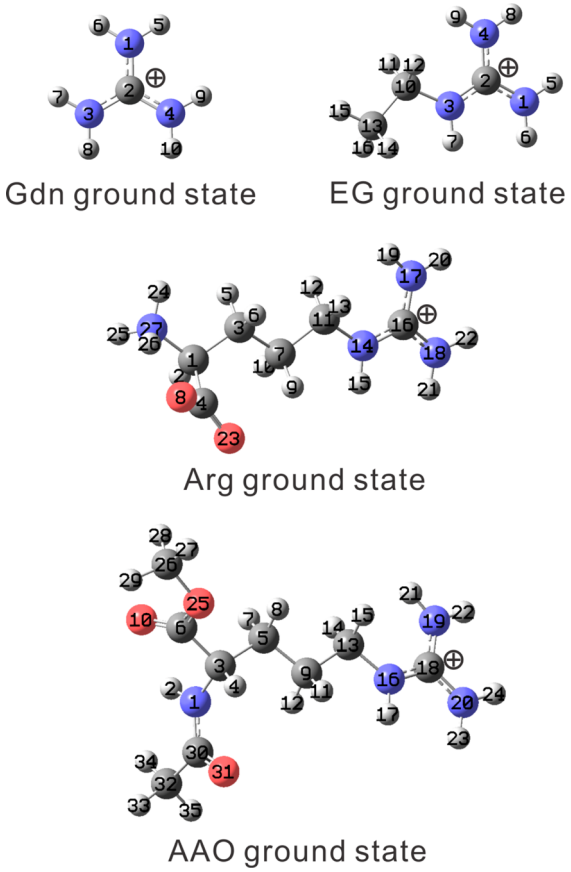

Figure 1. Calculated electronic ground state equilibrium geometries of Gdn, EG, Arg, and AAO.

We measured the 204 nm excited UVRR spectra of Gdn, EG, Arg, and AAO and used density functional theory (DFT) to calculate their electronic ground and first excited state conformations and their resonance Raman spectra. We also find that the ~1170 cm^{-1} Arg band is sensitive to the hydration of the Gdn group. We used this marker band to study the conformational dependence of the hydration of Arg in the peptides AP (sequence: $A_8RA_4RA_4RA_2$) and AEP (sequence: $A_9RA_3EA_4RA_2$).

EXPERIMENTAL SECTION

Materials. Guanidinium chloride (GC), ethylguanidinium sulfate (98%, EGS), L-arginine chloride (98%), sodium perchlorate (98%, $NaClO_4$), barium perchlorate (97%, $Ba(ClO_4)_2$), silver perchlorate (anhydrous, 97%, $AgClO_4$), and acetonitrile (spectrophotometric grade) were purchased from Sigma-Aldrich Co. and used as received. $Ba(ClO_4)_2$ and $AgClO_4$ are explosive; handle with care. Ac-Arg-OMe chloride (AAOC) was purchased from Bachem Americas, Inc. The AP ($A_8RA_4RA_4RA_2$, >95% purity) and AEP ($A_9RA_3EA_4RA_2$, >95% purity) peptides were synthesized by Anaspec Inc. D_2O (99.9%) was purchased from Cambridge Isotope Laboratories, Inc. Water (18.2 MΩ·cm) was purified by a NANOPURE Infinity ultrapure water purifier. The concentrations of Gdn, EG, Arg, and AAO for UVRR were 10 mM. 0.2 M $NaClO_4$ was added as an internal standard for each solution.

Synthesis of Ethylguanidinium Perchlorate and Ac-Arg-OMe Perchlorate. Due to the high charge density of sulfate and chloride anions, EGS and AAOC are insoluble in acetonitrile. We exchanged the sulfate and chloride counterions to perchlorate in order to make the compounds soluble.

To convert EGS and AAOC into ethylguanidinium perchlorate (EGPC) and Ac-Arg-OMe perchlorate (AAOPC), ~0.1 M $Ba(ClO_4)_2$ or ~0.1 M $AgClO_4$ was slowly added to the ~0.1 M EGS or ~0.1 M AAOC aqueous solutions to form insoluble $BaSO_4$ or AgCl, respectively. The suspension was centrifuged several times to remove the precipitate. The supernatant was collected and gently heated with stirring to evaporate the water. The resulting EGPC and AAOPC were very light yellow viscous ionic liquids at room temperature. The yellow color derived from impurities. The calculated yields were 93% and 105%, respectively. The fact that the yield was greater than 100% indicated that a small amount of water remained in AAOPC.

204 nm Excited UVRR Spectra. The UVRR instrumentation has been described in detail elsewhere.[31] Briefly, the 204 nm excitation beam, generated from the frequency mixing of the fundamental and the third harmonic of a Nd:YLF pumped Ti:Sapphire laser (Photonic Industries, Inc.), was directed to an open flow sample stream. The backscattered Raman light was collected and then dispersed using a partially subtractive double monochromator and finally detected by a liquid nitrogen cooled, Lumogen coated, back-thinned CCD camera (Princeton Instruments Spec-10:400B).

The Raman scattering cross section of a specific band is calculated by:

$$\sigma_S = \frac{\sigma_{IS} c_{IS} I_S \eta_{IS}}{c_S I_{IS} \eta_S} \quad (1)$$

where σ is the Raman scattering cross section, c represents the concentration, I is the integrated intensity of a specific band, and η is the instrument efficiency at the frequency of the specific Raman band. The subscript S denotes the sample, which is EG or AAO, while the subscript IS denotes the perchlorate internal standard. The instrument efficiencies at the sample band (η_S) and the internal standard band (η_{IS}) were assumed to be equal. The Raman scattering cross section of perchlorate was estimated to be 0.12×10^{-26} cm^2·$molecule^{-1}$·sr^{-1} at 204 nm excitation by extrapolating the Raman cross section measurement of Dudik et al.[32]

DFT Calculations. The electronic ground state equilibrium structures of Gdn, EG, Arg, and AAO, as well as their electronic ground state vibrational frequencies, were calculated at the B3LYP/aug-cc-pVTZ level in water using the polarizable continuum model (PCM) to model solvent effects with the Gaussian 09 package.[33] The calculated frequencies were not scaled. The potential energy distributions (PED) of the vibrational normal modes were calculated using a program that we wrote.[34−36] The force along a ground state vibrational normal coordinate in the first electronic excited state at the ground state equilibrium geometry is the negative of the first derivative of the first electronic excited state potential energy function with respect to the ground state normal coordinate at the ground state equilibrium geometry. These first electronic excited state forces at the ground state equilibrium geometry, the first electronic

dx.doi.org/10.1021/jp404030u | J. Phys. Chem. B 2013, 117, 7145−7156

excited state equilibrium geometries, and the vibrational frequencies of Gdn and EG were calculated by time-dependent DFT at the B3LYP/aug-cc-pVTZ level in water with the PCM using the Gaussian 09 package.[33] The atomic charges were calculated using the atoms-in-molecules (AIM) method using the Bader charge analysis program developed by Andri Arnaldsson, Wenjie Tang, and Graeme Henkelman from the University of Texas at Austin.[37−39]

RESULTS AND DISCUSSION

Vibrational Assignments. *Guanidinium.* Figure 2 shows the 204 nm excited UVRR spectra of Gdn, EG, Arg, and AAO in

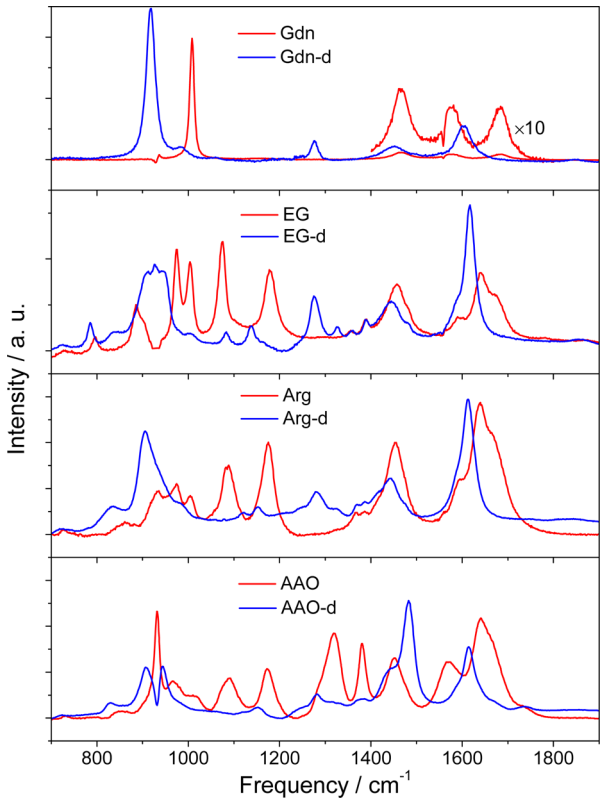

Figure 2. The 204 nm excited UVRR spectra of Gdn, EG, Arg, and AAO in both H_2O and D_2O.

both H_2O and D_2O. The Gdn UVRR spectra are very similar to those measured by Hudson and co-workers.[21] The spectrum of Gdn in H_2O shows a sharp intense CN_3 symmetric stretching band at 1008 cm^{-1} in addition to three weak, broad bands at ~1684 cm^{-1}, ~1578 cm^{-1}, and ~1466 cm^{-1}. The 1684 cm^{-1} and 1578 cm^{-1} bands result from the coupling between CN_3 asymmetric stretching and NH_2 scissoring vibrations.

For Gdn-d, the NH_2 hydrogen exchange for deuterium, causing the CN_3 asymmetric stretching and NH_2 scissoring vibrations to decouple and shift to 1604 cm^{-1} for the CN_3 asymmetric stretching and to 1278 cm^{-1} for ND_2 scissoring. The 1278 cm^{-1} band is resonance-enhanced due to a significant contribution from CN_3 symmetric stretching as discussed below.

Table 1 shows the calculated PED for the normal modes of Gdn and Gdn-d that contain at least 5% contributions from CN_3 stretching. The 1466 cm^{-1} Gdn band in H_2O and the 1451 cm^{-1} Gdn-d band in D_2O are assigned to the first overtone of the CN_3 out-of-plane deformation mode. The CN_3 out-of-plane deformation mode, calculated to be 727 cm^{-1} for Gdn or 709

Table 1. Gdn and Gdn-d Vibrational Normal Modes Involving at Least 5% Contribution from CN_3 Stretching

	exptl (cm^{-1})	calcd (cm^{-1})	PED[a] (%)
Gdn	1684	1694	N3−H_2 scs (40), N4−H_2 scs (40), N1−H_2 scs (12), **C2−N_3 s str (5)**
		1674	**C2−N_3 as str′ (39)**, N3−H_2 scs (26), N4−H_2 scs (26), C2−N3N4 rock (5)
		1673	N1−H_2 scs (45), **C2−N_3 as str (38)**, C2−N3N4 scs (5)
	1578	1592	**C2−N_3 as str (35)**, N1−H_2 scs (33), C2−N3N4 scs (11), N4−H_2 rock (7), N3−H_2 rock (7)
		1588	**C2−N_3 as str′ (35)**, N3−H_2 scs (21), N4−H_2 scs (21), C2−N3N4 rock (10), N1−H_2 rock (8)
		1126	N4−H_2 rock (35), N3−H_2 rock (35), **C2−N_3 as str (28)**
		1116	N1−H_2 rock (45), **C2−N_3 as str′ (27)**, N4−H_2 rock (13), N3−H_2 rock (12)
	1008	1023	**C2−N_3 s str (98)**
Gdn-d	1604	1602	**C2−N_3 as str′ (76)**, C2−N3N4 rock (12), N1−D_2 rock (5)
		1601	**C2−N_3 as str (75)**, C2−N3N4 scs (13)
	1278	1302	N3−D_2 scs (26), N4−D_2 scs (26), **C2−N_3 s str (26)**, N1−D_2 scs (21)
	919	920	**C2−N_3 s str (70)**, N1−D_2 scs (7)
		911	N4−D_2 rock (28), N3−D_2 rock (28), **C2−N_3 as str (17)**, **C2−N_3 s str (10)**, C2−N3N4 scs (8)
		909	N1−D_2 scs (43), **C2−N_3 as str′ (19)**, N4−D_2 rock (11), N3−D_2 rock (11), C2−N3N4 rock (9)

[a]as str: asymmetric stretching; s str: symmetric stretching; scs: scissoring; rock: rocking.

cm^{-1} for Gdn-d, is Raman inactive; however, its first overtone is Raman active. The small downshift of this Gdn-d band in D_2O indicates that this vibrational mode also contains a small contribution from ND_2 motions. In D_2O, the 919 cm^{-1} CN_3 symmetric stretching band downshifts from its 1008 cm^{-1} frequency in H_2O, confirming that CN_3 symmetric stretching is coupled to ND_2 scissoring.

Ethylguanidinium. Table 2 displays the PED for the normal modes of EG and EG-d. The EG UVRR spectra in both H_2O and D_2O show more features than the Gdn UVRR spectra because the ethyl group substitution breaks the Gdn symmetry. The CN_3 asymmetric stretching motion couples to NH_2 scissoring and a small amount of CN_2 rocking and/or CN_2 scissoring, giving rise to three moderately resolved bands at ~1674 cm^{-1}, ~1639 cm^{-1}, and ~1590 cm^{-1}. For EG-d, the CN_3 asymmetric stretching and ND_2 scissoring are decoupled, giving rise to a narrow 1617 cm^{-1} band with a shoulder at ~1588 cm^{-1}.

Hudson and co-workers[21] proposed that the overtone of the CN_3 out-of-plane deformation mode is Raman active in alkyl substituted Gdns. By comparing the ~1457 cm^{-1} band of EG and the ~1442 cm^{-1} band of EG-d with the 1466 cm^{-1} band of Gdn and the 1451 cm^{-1} band of Gdn-d, it is reasonable to assign these bands to the first overtones of the CN_3 out-of-plane deformation modes. This assignment is supported by the calculation, which gives fundamental frequencies of 728 cm^{-1} for EG and 720 cm^{-1} for EG-d. The methylene CH_2 scissoring band appears as a shoulder at ~1482 cm^{-1} in the spectra of both EG and EG-d. The bands at ~1389 cm^{-1} and ~1356 cm^{-1} show little frequency shift between EG and EG-d. Thus, these bands are assigned to the methyl CH_3 umbrella mode and the methylene CH_2 wagging. The band at 1180 cm^{-1} involving C10−N3 stretching is strongly

dx.doi.org/10.1021/jp404030u | J. Phys. Chem. B 2013, 117, 7145−7156

Table 2. EG and EG-d Vibrational Normal Modes Involving at Least 5% Contribution from CN_3 Stretching

	exptl (cm^{-1})	calcd (cm^{-1})	PED[a] (%)
EG	~1674	1689	N4−H_2 scs (46), N1−H_2 scs (32), **C2−N_3 as str (7)**, **C2−N_3 as str′ (5)**
		1673	N1−H_2 scs (35), **C2−N_3 as str′ (33)**, N4−H_2 scs (9), N3−H ipb (8), C2−N1N4 rock (5), **C2−N_3 as str (5)**
	1639	1644	**C2−N_3 as str (43)**, N1−H_2 scs (16), N3−H ipb (15), C2−N1N4 scs (7), N4−H_2 scs (6), N4−H_2 rock (46)
	1590	1603	N4−H_2 scs (33), **C2−N_3 as str (16)**, **C2−N_3 as str′ (16)**, N3−H ipb (11), N1−H_2 rock (8), C2−N1N4 rock (6), C2−N1N4 scs (5)
		1457	N3−H ipb (36), **C2−N_3 as str′ (20)**, C10−H_2 wag (18)
		1381	C10−H_2 wag (66), N3−H ipb (13), **C2−N_3 as str′ (5)**, C13−H_3 s def (5)
	1180	1180	N3−C10 str (47), C13−H_3 rock′ (12), N1−H_2 rock (9), **C2−N_3 s str (8)**
		1141	N4−H_2 rock (22), C13−H_3 rock′ (15), C10−C13 str (10), **C2−N_3 as str (9)**, C10−C13N3 scs (9), N1−H_2 rock (7), **C2−N_3 s str (5)**, C13−H_3 rock (5), **C2−N_3 as str′ (5)**
	1075	1084	**C2−N_3 s str (33)**, N1−H_2 rock (27), **C2−N_3 as str (13)**, C10−C13 str (10), N3−C10 str (9)
		1070	N4−H_2 rock (45), N1−H_2 rock (33), **C2−N_3 as str′ (6)**, C13−H_3 rock′ (5)
	975	1016	C10−C13 str (58), **C2−N_3 s str (31)**, N3−C10 str (5)
		907	C13−H_3 rock′ (24), N3−C10 str (19), **C2−N_3 s str (11)**, N3−C2C10 ipb (10), C13−H_3 rock (9), C10−H_2 wag (6), C2−N1N4 rock (6)
EG-d	1617	1612	**C2−N_3 as str (68)**, C2−N1N4 scs (11)
	~1585	1593	**C2−N_3 as str′ (68)**, C2−N1N4 rock (14)
	1326	1307	N1−D_2 scs (34), **C2−N_3 s str (28)**, N4−D_2 scs (14), N3−D ipb (12), N3−C10 str (5)
	945	956	N3−D ipb (44), **C2−N_3 s str (32)**, N3−C10 str (6), C13−H_3 rock′ (5), N4-D_2 scs (5)
	913	910	N4−D_2 rock (26), N1−D_2 rock (24), **C2−N_3 as str (16)**, **C2−N_3 s str (16)**, C2−N1N4 rock (7)
		899	C13−H_3 rock′ (20), N3−C10 str (14), N4−D_2 rock (11), **C2−N_3 s str (9)**, N3−C2C10 ipb (9), C2−N1N4 rock (8), C13−H_3 rock (7), C10−H_2 wag (5)
	785	813	N1−D_2 rock (46), N4−D_2 rock (25), N3−C10 str (8), **C2−N_3 s str (5)**

[a]as str: asymmetric stretching; s str: symmetric stretching; scs: scissoring; rock: rocking; wag: wagging; twist: twisting; ipb: in-plane bending; s def: symmetric deformation.

Table 3. Arg amd Arg-d Vibrational Normal Modes Involving at Least 5% Contribution from CN_3 Stretching

	exptl (cm^{-1})	calcd (cm^{-1})	PED[a] (%)
Arg	~1667	1686	N17−H_2 scs (54), N18−H_2 scs (25), **C16−N_3 as str (6)**, **C16−N_3 as str′ (6)**
		1672	N18−H_2 scs (37), **C16−N_3 as str′ (32)**, N14−H ipb (8), N17−H_2 scs (7), **C16−N_3 as str (6)**, C16−N17N18 rock (5)
	1640	1643	**C18−N_3 as str (46)**, N18−H_2 scs (17), N14−H ipb (12), C16−N17N18 scs (8), N17−H_2 rock (5)
	1596	1598	N17−H_2 scs (32), **C16−N_3 as str′ (18)**, N14−H ipb (13), **C16−N_3 as str (11)**, C16−N17N18 rock (7), N18−H_2 rock (7), N18−H_2 scs (6)
		1459	N14−H ipb (30), C11−H_2 wag (29), **C16−N_3 as str′ (17)**
	1176	1167	N14−C11 str (25), N18−H_2 rock (12), **C16−N_3 s str (10)**, N27−H_3 rock′ (8), N17−H_2 rock (7), **C16−N_3 as str (6)**, C1−C3 str (5)
	1085	1084	**C16−N_3 s str (18)**, N17−H_2 rock (17), **C16−N_3 as str (12)**, N14−C11 str (7), N18−H_2 rock (7), N27−H_3 rock (5), C3−C7 str (5)
		1072	N18−H_2 rock (36), N17−H_2 rock (15), **C16−N_3 s str (8)**, C7−C11 str (7), C3−C7 str (7)
	975	1005	C1−N27 str (20), **C16−N_3 s str (16)**, C1−C3 str (15), N27−H_3 rock′ (10), N14−C11 str (6)
		966	C1−N27 str (22), **C16−N_3 s str (22)**, N14−C11 str (13), C3−C7 str (12), C7−C11 str (7)
Arg-d	1612	1613	**C16−N_3 as str (70)**, C16−N17N18 scs (11)
	~1586	1593	**C16−N_3 as str′ (70)**, C16−N17N18 rock (14)
	1279	1314	N18−D_2 scs (17), **C16−N_3 s str (17)**, C3−H_2 wag (16), C7−H_2 wag (13), N17−D_2 scs (8), N14−D ipb (8)
		1297	C1−H rock′ (22), C7−H_2 wag (19), C3−H_2 wag (13), N18−D_2 scs (7), C11−H_2 wag (5), C11−H_2 twist (5), **C16−N_3 s str (5)**
		1294	C1−H rock′ (20), C1−H rock (13), C11−H_2 twist (11), C7−H_2 twist (7), N18−D_2 scs (7), C3−H_2 rock(6), C7−H_2 wag (5), **C16−N_3 s str (5)**
		942	C1−N27 str (18), C1−C4 str (10), **C16−N_3 s str (9)**, N14−D ipb (8), C11−H_2 rock (6), C3−H_2 rock (5)
	907	926	**C16−N_3 s str (31)**, C1−N27 str (9), N17−D_2 rock (6), C3−C7 str (6)
		907	N17−D_2 rock (28), N18−D_2 rock (24), **C16−N_3 as str (16)**, **C16−N_3 s str (15)**, C16−N17N18 scs (7)

[a]as str: asymmetric stretching; s str: symmetric stretching; scs: scissoring; rock: rocking; wag: wagging; twist: twisting; ipb: in-plane bending.

resonance enhanced as shown below. This band is sensitive to the environment of the Gdn group.

In EG and EG-d, the CN_3 symmetric stretching motion is distributed over several bands. We are unable to unambiguously assign the bands below 1100 cm^{-1}.

Arginine. The Arg and Arg-d PED for its vibrational normal modes are given in Table 3. The UVRR spectra of Arg and Arg-d are very similar to those of EG and EG-d; however, the Arg bands are somewhat broader than those of EG and EG-d. Similar to the 1180 cm^{-1} band in EG, the ~1175 cm^{-1} band involving C13−N16 stretching is well-resolved in the UVRR spectra of Arg. The bands below 1000 cm^{-1} differ significantly from those of EG.

N-Acetyl Arginine Methyl Ester. The PED for the vibrational normal modes of AAO and AAO-d are shown in Table 4. In addition to enhancement of Arg vibrations, the AAO and AAO-d UVRR spectra show enhancement of amide vibrations because the amide $\pi-\pi^*$ electronic transition is also in resonance with 204 nm excitation. The AmI band overlaps with the Gdn group

dx.doi.org/10.1021/jp404030u | J. Phys. Chem. B 2013, 117, 7145−7156

Table 4. AAO and AAO-d Vibrational Normal Modes Involving at Least 5% Contribution from CN_3 Stretching

	exptl (cm^{-1})	calcd (cm^{-1})	PED[a] (%)
AAO		1692	N19−H_2 scs (50), N20−H_2 scs (28), **C18−N_3 as str (6)**, **C18−N_3 as str′ (5)**
		1673	N20−H_2 scs (39), **C18−N_3 as str′ (31)**, N19−H_2 scs (8), N16−H ipb (7), **C18−N_3 as str (6)**, C18−N19N20 rock (5)
		1644	**C18−N_3 as str (43)**, N16−H ipb (16), N20−H_2 scs (15), C18−N19N20 scs (7), N19−H_2 scs (6), N19−H_2 rock (5)
		1605	N19−H_2 scs (29), **C18−N_3 as str′ (17)**, **C18−N_3 as str (17)**, N16−H ipb (11), N20−H_2 rock (8), C18−N19N20 rock (6), C18−N19N20 scs (5),
		1461	N16−H ipb (32), C13−H_2 wag (23), **C18−N_3 as str′ (19)**
	1170	1170	N16−C13 str (39), N20−H_2 rock (8), **C18−N_3 s str (13)**, N19−H_2 rock (8), **C18−N_3 as str (7)**
	1091	1084	**C18−N_3 s str (29)**, N20−H_2 rock (29), **C18−N_3 as str (11)**, C9−C13 str (10), N16−C13 str (6)
	∼1018	1005	C26−O25 str (29), C3−C6 str (18), C3−C5 str (14), **C18−N_3 s str (6)**
		990	C26−O25 str (14), C30−C32 str (11), N1−C3C30 ipb (8), C6−C3−N1 def (6), **C18−N_3 s str (6)**, C30−N1 str (6), C30−O31 ipb (5)
	966	973	**C18−N_3 s str (22)**, N16−C13 str (12), C5−C9 str (10), C26−O25 str (6), C9−C13 str (6), C3−C6 str (5)
AAO-d	1617	1612	**C18−N_3 as str (69)**, C18−N19N20 scs (11)
		1593	**C18−N_3 as str′ (68)**, C18−N19N20 rock (14)
	1282	1308	N20−D_2 scs (25), **C18−N_3 s str (20)**, N19−D_2 scs (11), C3−H rock (10), N16−D ipb (8), N16−C13 str (5), C13−H_2 twist (5)
	944	935	**C18−N_3 s str (23)**, N1−D ipb (21), C30−N1 str (9), C32−H3 rock′ (5)
		931	**C18−N_3 s str (23)**, N1−D ipb (16), C30−N1 str (12), C32−H3 rock′ (5)
	907	910	N19−D_2 rock (31), N20−D_2 rock (22), **C18−N_3 as str (16)**, **C18−N_3 s str (1)**, C18−N19N20 scs (7)

[a]as str: asymmetric stretching; s str: symmetric stretching; scs: scissoring; rock: rocking; wag: wagging; twist: twisting; ipb: in-plane bending; def: deformation.

CN_3 asymmetric stretching band. The AmII band appears at ∼1570 cm^{-1}. The band at 1452 cm^{-1} in AAO and the shoulder appearing at ∼1435 cm^{-1} in AAO-d are assigned to the overtones of the CN_3 out-of-plane deformation modes. The narrow band at 1381 cm^{-1} originates from the coupling of the methyl CH_3 bending mode of the acetyl group with the N−H bending mode of the amide bond. The AmIII band occurs at 1319 cm^{-1}. The AAO 1170 cm^{-1} band that involves C13−N16 stretching is well-resolved in the UVRR spectrum. This band is equivalent to the 1180 cm^{-1} band of EG and is also sensitive to the Gdn group environment.

For AAO-d, the AmI, AmII, and AmIII bands disappear, while the AmII′ band (C−N stretching) appears at 1483 cm^{-1}, revealing the CN_3 asymmetric stretching at 1617 cm^{-1}. The weak, broad bump at ∼1376 cm^{-1} is probably an overlapping methylene CH_2 wagging band.

Calculated Electronic Ground State Structures of Gdn and EG. The calculated electronic ground state equilibrium geometry of Gdn in water has C_2 symmetry, which is different from those geometries calculated in the gas phase.[40,41] Gobbi and Frenking examined the electronic structure of Gdn and concluded that the resonance stabilization of Gdn is not strong enough to constrain the molecule to have D_{3h} symmetry.[41]

The calculated Gdn group electronic ground state geometry of EG is similar to that of Gdn; however, in EG the C2−N3 bond is 0.001 Å shorter, while the C2−N1 and C2−N4 bonds are 0.005 Å and 0.002 Å longer than the corresponding C−N bonds of Gdn (Table 5). The shortening of the C2−N3 bond is due to electron release by the adjacent ethyl group, allowing the positive charge on the Gdn group to extend into the ethyl group (Table 6).

The sp^2 hybridization of the N3 nitrogen atom requires the C2, N3, H7, and C10 atoms to be planar; however, the N3, H7, C10, and C13 atoms are not planar due to the sp^3 hybridization of the C10 carbon atom.

We calculated the effect of changing the torsion angle of the C13−C10−N3−C2 linkage on the energy of EG using DFT. The calculated potential energy surface along the C13−C10−N3−C2 torsion angle (Figure 3) is consistent with a previous report[42] that indicated the trans-conformation (180°) is the global energy minimum. Two local minima corresponding to ±90° conformations exist 2.4 kJ·mol^{-1} above the global minimum. At 298 K, with the thermal energy correction, which corrects the Gibbs free energy by accounting for the molecular translational energy, rotational energy, and vibrational energy at 298 K and 1 atm, the energy gap is 6.6 kJ·mol^{-1}. The population fractions of these three conformers are calculated from the Boltzmann distribution to be 0.88, 0.06, and 0.06, respectively. Based on these calculations, EG likely occurs in a conformational distribution. The low energy barriers of ∼5 kJ·mol^{-1} (Figure 3, with thermal energy correction at 298 K and 1 atm, the barrier is ∼9 kJ·mol^{-1}) suggest fast transitions between the conformers.

Table 5. Calculated Bond Lengths of Gdn and EG in the Ground and First Excited States[a]

	bond length	ground state (Å)	excited state (Å)	difference (Å)
Gdn	C2−N1	1.3305	1.3654	0.0349
	C2−N3	1.3305	1.4085	0.0780
	C2−N4	1.3305	1.4085	0.0780
EG	C2−N1	1.3353	1.4101	0.0748
	C2−N3	1.3291	1.3650	0.0359
	C2−N4	1.3325	1.4110	0.0785
	N3−C10	1.4672	1.4655	−0.0017
	C10−C13	1.5192	1.5198	0.0006

[a]Bond lengths are calculated at B3LYP/aug-cc-pVTZ level using Gaussian 09 package.

Calculated First Electronic Excited State Structure of EG. The equilibrium geometry displacement of the first electronic excited state and the first electronic excited state force along each vibrational normal coordinate of the electronic ground state at the ground state equilibrium geometry are related to the Raman scattering cross section as shown below. Generally, along a vibrational normal coordinate, the larger the vertical transition first electronic excited state force, or the larger the nuclear displacement of the first electronic excited state equilibrium geometry from the electronic ground state

dx.doi.org/10.1021/jp404030u | J. Phys. Chem. B 2013, 117, 7145−7156

Table 6. Calculated Atomic Charges of Gdn and EG in the Ground and First Excited States[a]

	atom	ground state	excited state	difference
Gdn	N1	−1.18	−1.07	0.11
	C2	1.68	1.21	−0.47
	N3	−1.22	−0.97	0.25
	N4	−1.22	−0.97	0.25
	H5	0.48	0.45	−0.03
	H6	0.48	0.45	−0.03
	H7	0.50	0.47	−0.03
	H8	0.48	0.49	0.01
	H9	0.49	0.48	−0.01
	H10	0.48	0.47	−0.01
EG	N1	−1.22	−0.97	0.25
	C2	1.69	1.17	−0.52
	N3	−1.16	−1.07	0.09
	N4	−1.19	−0.96	0.23
	H5	0.48	0.45	−0.03
	H6	0.49	0.49	0.00
	H7	0.45	0.45	0.00
	H8	0.48	0.48	0.00
	H9	0.47	0.47	0.00
	C10	0.36	0.46	0.10
	H11	0.02	0.04	0.02
	H12	0.03	0.02	−0.01
	C13	0.00	0.05	0.05
	H14	0.02	0.00	−0.02
	H15	0.04	0.02	−0.02
	H16	0.03	−0.01	0.04

[a]The atomic charges were calculated by using the Bader program developed by Andri Arnaldsson, Wenjie Tang, and Graeme Henkelman at The University of Texas at Austin; http://theory.cm.utexas.edu/vtsttools/bader/.

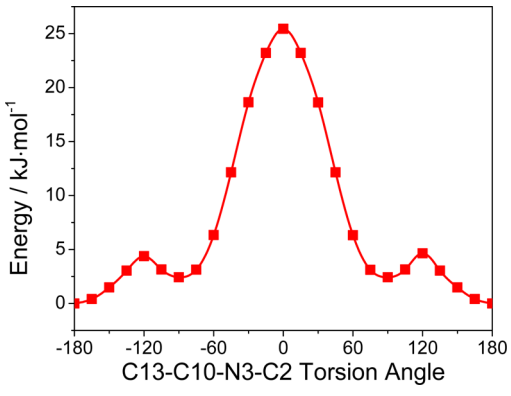

Figure 3. Calculated EG potential energy surface along the C13−C10−N3−C2 torsion angle.

equilibrium geometry, the larger the corresponding vibrational mode resonance Raman scattering cross section.

In order to elucidate the resonance Raman enhancement mechanism of the EG vibrations, we calculated the first electronic excited state equilibrium geometry of EG and the first electronic excited state force along each vibrational normal coordinate of the electronic ground state at the electronic ground state equilibrium geometry using the time-dependent DFT method in the Gaussian 09 software package, as described above in the Experimental section.

The equilibrium geometry of the first electronic excited state of EG significantly differs from that of the electronic ground state. The C2−N3 bond length increases by 0.036 Å (2.7%); the C2−N1 bond increases by 0.075 Å (5.6%), and the C2−N4 bond increases by 0.078 Å (5.9%) (Table 5). The elongations of these CN bonds are presumably responsible for the large resonance Raman enhancement of the CN_3 stretching vibrations (Figure 4) in the UVRR spectra of EG. Tables 1−4 list those vibrations that involve more than 5% CN_3 stretching contributions for Gdn, EG, Arg, and AAO.

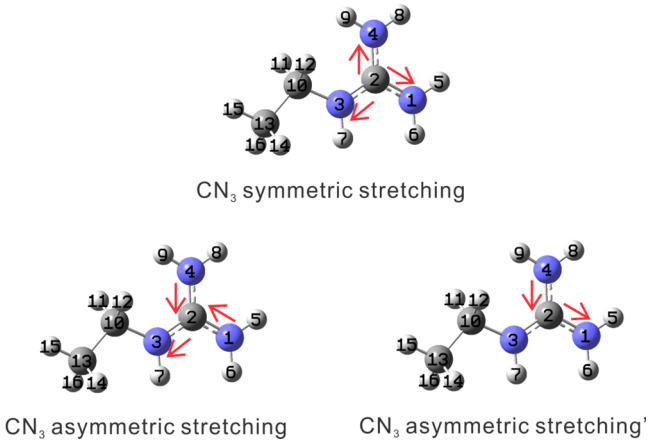

Figure 4. Definitions of CN_3 stretching vibrations in EG, Arg, and AAO.

Table 6 shows the calculated atomic charges of EG in both the electronic ground and first excited states. The atomic charge differences between the electronic ground and first excited states clearly indicate that significant electron transfers occur between the electronic ground state and the first electronic excited state. This electron transfer causes the pyramidalization of the central carbon atom, which is consistent with the previous calculations for Gdn by Hudson and co-workers using the semiempirical INDO/S method.[21] Also, the first electronic excited state structure of AB_3 molecules was first examined and predicted to be somewhat pyramidal by Walsh in the 1950s.[43]

In the electronic ground state, the C2 carbon atom is sp^2 hybridized, and the perpendicular p orbital of the C2 carbon overlaps with the three p orbitals of the three nitrogen atoms. In the first electronic excited state, the C2 carbon atom carries more electron density. This increased electron density of the C2 carbon in the excited state causes orbital rehybridization from sp^2 to sp^3-like, which results in pyramidalization. The sp^3-like hybridization of the central C2 carbon atom also explains the elongations of the three Gdn group CN bonds; σ bonds involving sp^3 hybridized orbitals are longer than those involving sp^2 hybridized orbitals.

The pyramidalization of the C2 carbon in the first excited state results in a nonplanar CN_3 geometry that gives rise to a large displacement along the CN_3 out-of-plane deformation normal coordinate. The overtone of this CN_3 out-of-plane deformation appears as a strong band in all compounds studied here. Recently, we studied the excitation profiles of Arg and found that the overtone of the CN_3 out-of-plane vibration is enhanced as the excitation wavelength is tuned into resonance.[30]

Figure 5 shows the calculated EG first electronic excited state structure and HOMOs. In the first electronic excited state, the C2−N1 and C2−N4 bonds are elongated more than the C2−N3 bond (Table 5). The elongations of these bonds diminish the overlap of the two perpendicular p orbitals of the N1 and N4 nitrogen atoms with the p orbital of the C2 carbon. The C2−N1

dx.doi.org/10.1021/jp404030u | J. Phys. Chem. B 2013, 117, 7145−7156

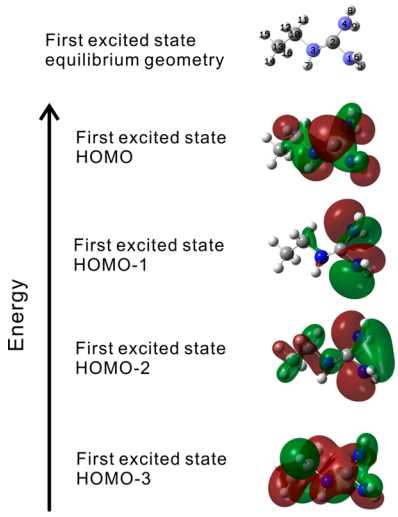

Figure 5. Calculated structure and molecular orbitals of EG in the first electronic excited state.

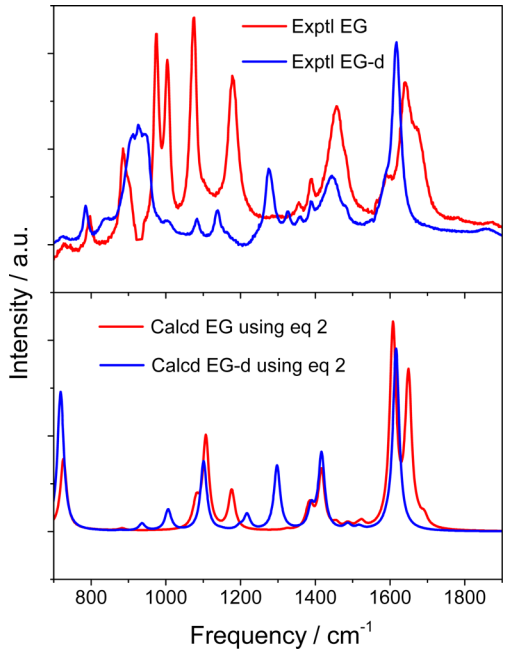

Figure 6. 204 nm excited UVRR spectra of EG and EG-d (top panel) and calculated resonance Raman spectra of EG and EG-d (bottom panel). The calculated spectra are the weighted average, based on the population fraction of each conformer, of the calculated spectra of the three EG conformers. See text for more details.

and C2−N4 bonds rotate by ~90° (Figure 5), enabling the two p orbitals to partially overlap; however, the two nitrogen atoms are too far away from each other (2.247 Å) to form a normal σ bond. The resulting overlap is not as efficient as the overlap of the C2−N3 p orbitals with normal π-bond character. Therefore, the molecular orbital of this N1−N4 "σ bond" has a higher energy than that of the C2−N3 normal π-bond. The four molecular orbitals formed from the four p orbitals (one from the central carbon and three from the nitrogen atoms) in the first electronic excited state occur in an increasing energy order: the bonding π-orbital between the C2 carbon and the N3 nitrogen, the in-phase overlap between the N1 and N4 nitrogen p orbitals, the out-of-phase overlap between the N1 and N4 nitrogen p orbitals, and the antibonding π-orbital between the C2 carbon and the N3 nitrogen.

Calculation of the UVRR Spectra of EG and EG-d. Using time-dependent Raman theory,[44−47] under the Born−Oppenheimer approximation and the short time dynamics approximation, Heller et al. predicted that, for the resonance and preresonance Raman cases, the square of the Raman polarizability of the kth vibrational normal mode, $|\alpha_k|^2$, is proportional to the square of the force (V_k) on the first electronic excited state potential energy surface along that particular vibrational normal coordinate k at the electronic ground state equilibrium geometry. The Raman scattered intensity also increases with the excitation frequency to the fourth power, $\omega_I(\omega_I - \omega_k)^3$:

$$I_k \sim \omega_I(\omega_I - \omega_k)^3 \frac{V_k^2}{\omega_k} \quad (2)$$

where ω_I and ω_k are the excitation frequency and the kth vibrational frequency, respectively. Using eq 2, the relative resonance Raman intensity of each vibrational normal mode of EG and EG-d was calculated from the first electronic excited state force along each vibrational normal mode that was obtained from DFT and TD-DFT calculations. Assuming a Lorentzian band shape with a FWHM of 20 cm^{-1} for each mode, the resonance Raman spectra of EG and EG-d were calculated and are shown in the bottom panel of Figure 6. For comparison, the experimental spectra are shown in the top panel of Figure 6.

The calculated spectra from eq 2 moderately agree with those measured. In the calculated spectra, the bands involving CN_3 asymmetric stretching between 1500 cm^{-1} and 1700 cm^{-1} and the bands involving CN_3 symmetric stretching between 900 cm^{-1} and 1200 cm^{-1} are resonance-enhanced, which is expected from the calculated large bond length increase along the three CN bonds of the Gdn group.

The experimentally observed 1466 cm^{-1} EG and 1451 cm^{-1} EG-d overtone bands are missing in the calculated spectra. Equation 2 only describes the fundamental vibrational band intensities and intrinsically does not include overtone or combination band intensities. It is evident from Figure 6 that the 1180 cm^{-1} band, which involves C10−N3 stretching, is resonance-enhanced. From our experimental UVRR spectra, we find that this band can be used to determine the hydration state of the Arg side chains in peptides and proteins, as discussed below.

If no vibrational frequency change or Duschinsky rotation occurs between the electronic ground state and the first excited state, it is straightforward to rewrite eq 2 as:

$$I_k \sim \omega_I(\omega_I - \omega_k)^3(\omega_k^2\Delta_k^2) \quad (3)$$

where Δ_k is the displacement of the equilibrium geometry of the first electronic excited state from the electronic ground state along the kth dimensionless vibrational normal coordinate. Equation 3 is widely used in the interpretation and prediction of resonance Raman spectra. For Gdn and Gdn-d, the strongly resonance enhanced ground state CN_3 symmetric stretching vibration remains almost identical to that in the first electronic excited state (Table 7). Thus eq 3 is valid to analyze the enhancement of this particular mode. However, for EG and EG-d, the excited state vibrational normal modes change significantly from those of the ground state, indicating that a significant Duschinsky rotation is occurring for these vibrations (Table 8). Obviously the first electronic excited state vibrational frequencies will differ from those in the electronic ground state. Therefore,

dx.doi.org/10.1021/jp404030u | J. Phys. Chem. B 2013, 117, 7145−7156

Table 7. First Electronic Excited State Gdn and Gdn-d Vibrational Normal Modes Involving at Least 5% Contribution from CN_3 Stretching

	exptl (cm^{-1})	calcd (cm^{-1})	PED[a] (%)
EG		1631	N1−H_2 scs (69), **C2−N_3 as str (10)**, N4−H_2 scs (8)
		1469	**C2−N_3 as str (59)**, H7−N3−C2−N4 tor (12), N1−H_2 scs (6), C2−N3N4 scs (6), H10−N4−C2−N1 tor (6)
		1243	C2−N3N4 rock (35), N1−H_2 rock (27), **C2−N_3 as str′ (21)**, C2−N_3 def (9)
		1035	**C2−N_3 as str′ (44)**, N1−H_2 rock (20), H7−N3−C2−N4 tor (11), H10−N4−C2−N1 tor (7), N4−H_2 rock (5)
		933	**C2−N_3 s str (66)**, H10−N4−C2−N1 tor (19), C2−N_3 s def (7)
EG-d		1485	**C2−N_3 as str (65)**, D7−N3−C2−N4 tor (12), C2−N3N4 scs (5), D10−N4−C2−N1 tor (5), N1−D_2 scs (5)
		1256	**C2−N_3 as str′ (25)**, N4−D_2 scs (24), N3−D_2 scs (24), C2−N3N4 rock (11), D7−N3−C2−N4 tor (6)
		1090	C2−N3N4 rock (35), **C2−N_3 as str′ (17)**, C2−N_3 def (9), N4−D_2 scs (9), N3−D_2 scs (9), D10−N4−C2−N1 tor (9), N1−D_2 rock (8)
		975	C2−N_3 def (35), N4−D_2 rock (23), D10−N4−C2−N1 tor (11), D7−N3−C2−N4 tor (10), N3−D_2 rock (9), **C2−N_3 s str (5)**
		850	N1−H_2 rock (42), **C2−N_3 as str′ (21)**, D10−N4−C2−N1 tor (10), C2−N3N4 rock (8), D7−N3−C2−N4 tor (5)
		842	**C2−N_3 s str (61)**, N4−D_2 rock (16), N3−D_2 rock (7)

[a]as str: asymmetric stretching; s str: symmetric stretching; scs: scissoring; rock: rocking; wag: wagging; twist: twisting; ipb: in-plane bending; as def: asymmetric deformation; s def: symmetric deformation; tor: torsion.

Table 8. First Electronic Excited State EG and EG-d Vibrational Normal Modes Involving at Least 5% Contribution from CN_3 Stretching

	exptl (cm^{-1})	calcd (cm^{-1})	PED[a] (%)
EG		1542	**C2−N_3 as str (41)**, N3−H ipb (31), H9−N4−C2−N1 tor (7)
		1430	N3−H ipb (28), **C2−N_3 as str (28)**, C10−H_2 wag (21)
		1378	C10−H_2 wag (59), N3−H ipb (15), **C2−N_3 as str (5)**, C13−H_3 s def (5)
		1185	C10−H_2 rock (19), **C2−N_3 as str′ (17)**, C13−H_3 rock′ (17), C2−N1N4 rock (9), N3−C10 str (9), N3−C2C10 ipb (8)
		1113	**C2−N_3 as str′ (52)**, N3−C10 str (21), **C2−N_3 s str (6)**
		1065	C10−C13 str (33), **C2−N_3 as str′ (18)**, N3−C10 str (16), C13−H_3 rock′ (6), **C2−N_3 s str (6)**, C2−N1N4 rock (5), N3−H ipb (5)
		971	**C2−N_3 s str (41)**, C10−C13 str (33), C13−H_3 rock′ (7)
		884	C13−H_3 rock′ (25), **C2−N_3 s str (22)**, N3−C10 str (15), N3−C2C10 ipb (9)
EG-d		2104	D9−N4−C2−N1 tor (47), D6−N1−C2−N4 tor (16), N1−C2D5D6 s def (7), **C2−N_3 s str (5)**
		1511	C10−H_2 scs (66), C13−H_3 as def′ (12), **C2−N_3 as str (5)**
		1500	**C2−N_3 as str (59)**, D9−N4−C2−N1 tor (8), C13−H_3 as def (6), N3−C10 str (5), N3−D ipb (5)
		1486	C13−H_3 as def (77), C10−H_2 scs (8), C13−H_3 rock (7), **C2−N_3 as str (5)**
		1241	N1−D_2 scs (63), **C2−N_3 s str (9)**, **C2−N_3 as str′ (6)**, N4−D_2 scs (5), D6−N1−C2−N4 tor (5)
		1057	**C2−N_3 as str′ (31)**, N1−D_2 scs (14), N3−C10 str (12), C10−C13 str (11), N4−D_2 scs (7), C2−N1N4 rock (7), D6−N1−C2−N4 tor (5)
		997	C10−C13 str (26), **C2−N_3 s str (15)**, N1−D_2 rock (8), N1−C2D5D6 s def (7), N4−D_2 rock (7), **C2−N_3 as str′ (6)**, D9−N4−C2−N1 tor (6), D6−N1−C2−N4 tor (6), N3−D ipb (5)
		964	H6−N1−C2−N4 tor (24), N4−D_2 rock (14), N4−D_2 rock (12), D9−N4−C2−N1 tor (9), C2−N_3 s def (9), C10−C13 str (6), **C2−N_3 as str′ (5)**, N1−C2D5D6 s def (5)
		896	N3−D ipb (27), C13−H_3 rock′ (24), N3−C10 str (19), **C2−N_3 s str (5)**
		842	**C2−N_3 s str (31)**, C13−H_3 rock′ (12), C10−H_2 rock (6), **C2−N_3 as str′ (6)**, N3−C2C10 ipb (5), N4−D_2 rock (5)

[a]as str: asymmetric stretching; s str: symmetric stretching; scs: scissoring; rock: rocking; wag: wagging; twist: twisting; ipb: in-plane bending; as def: asymmetric deformation; s def: symmetric deformation; tor: torsion.

the applicability of eq 3 for EG and EG-d to interpret resonance Raman spectra becomes questionable.

UVRR Spectra of EG in Water and in Acetonitrile. To study the effect of the environment on the UVRR spectrum of the Arg side chains, we examined the 204 nm excited UVRR spectra of EGPC in water and in acetonitrile (Figure 7a). Most of the bands in acetonitrile are significantly more intense than those in water. To understand this phenomenon, we measured the UV absorbance spectra of EG in both water and acetonitrile (Figure 7b) and found only small differences. The difference spectrum shows an additional weak, broad band at ∼200 nm. At 204 nm, the absorbance of EG in acetonitrile is about 15% greater than that in water.

The Raman band frequencies of EG in acetonitrile are slightly downshifted compared to those in water. Particularly, the 1180 cm^{-1} band in water downshifts to 1174 cm^{-1} in acetonitrile. This Arg side chain band occurs in a region that generally does not overlap with the amide vibrational bands in the UVRR spectra of proteins and peptides. Thus, this band can be conveniently used to probe the local environment and hydrogen bonding state of the Arg side chains. The other Arg side chain bands, such as the CN_3 asymmetric stretching bands between 1500 cm^{-1} to 1700 cm^{-1}, unfortunately, are overlapped by amide bands.

Our observed frequency increase of the UVRR 1174 cm^{-1} band of EG in acetonitrile to 1180 cm^{-1} in water is consistent with the IR study of Braiman et al.[48] With acetate as a counterion, they observed a higher frequency for this band in nonpolar solvents than in polar solvents, such as H_2O, methanol, and DMSO. The 1174 cm^{-1} band has contributions from the Gdn group NH_2 bending vibrations (Table 2). The hydrogen bond between the Gdn NH_2 and the hydrogen bonding acceptor molecule makes the NH_2 group more difficult to bend and

dx.doi.org/10.1021/jp404030u | J. Phys. Chem. B 2013, 117, 7145−7156

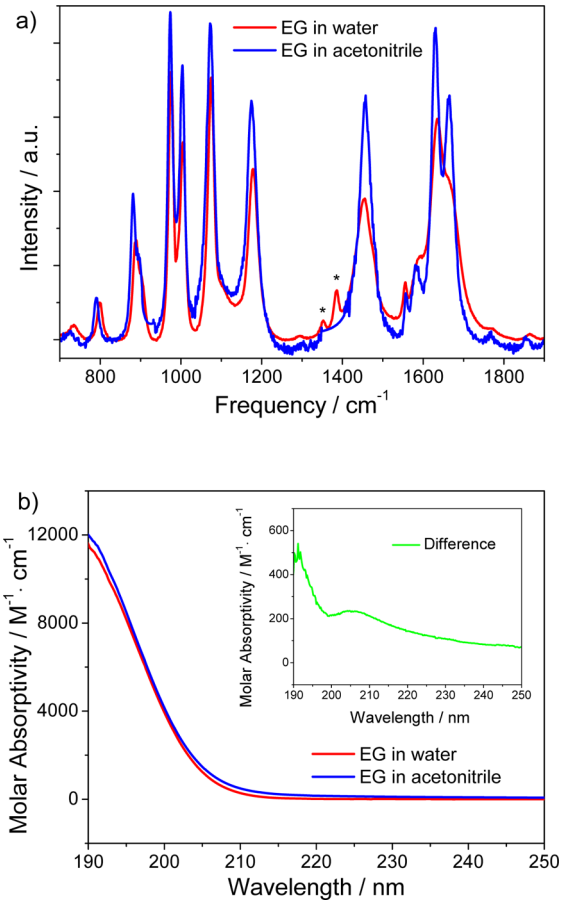

Figure 7. (a) 204 nm excited UVRR spectra and (b) UV absorbance spectra of EG in water and in acetonitrile. The bands marked with an asterisk in the spectrum of EG in water are missing in the spectrum of EG in acetonitrile due to the subtraction of the solvent.

narrows the potential well, thus increasing the bending force constant. Therefore, stronger NH_2 hydrogen bonding would upshift the frequency of this band.[49] Acetate is a strong hydrogen bond acceptor and can form a strong hydrogen bond with the EG NH_2 in nonpolar solvents resulting in an increased frequency of the 1174 cm^{-1} band. Therefore, the higher frequency observed in nonpolar solvents compared to polar solvents is due to the interaction of EG with the acetate counterion, not due to the decreased interaction with the nonpolar solvent molecules themselves.

In polar solvents, they observed a lower frequency of this band compared to nonpolar solvents because the polar solvent molecules form weaker hydrogen bonds with the EG NH_2 than does the acetate counterion. Since large numbers of polar solvent molecules are present, they compete with the acetate counterions and prevent the acetate from forming hydrogen bonds with the EG NH_2. Therefore, the lower frequencies they observed in polar solvents most likely reflect the weaker hydrogen bonding between the polar solvent molecules and the EG NH_2. These arguments are supported by the fact that the frequency dependence of this band on the identity of the counterion only occurs in the solid state or in nonpolar solvents, while in polar solvents this dependence disappears.[48]

In our experiment, the perchlorate counterion is a weak hydrogen bond acceptor and is expected to have little interaction with the EG NH_2 in either water or acetonitrile; thus, it has little impact on the EG frequency even in the less polar acetonitrile solvent. Therefore, the frequency shift of the 1174 cm^{-1} band observed here reflects the differences in the interactions of EG with water and acetonitrile.

Hydration of Guanidinium Group. We measured the 204 nm excited UVRR spectra of EG and AAO in different water–acetonitrile mixtures. For EG, as the water mole fraction increases, the frequency upshifts from 1174 cm^{-1} to 1180 cm^{-1}, while the cross section monotonically decreases from 6.5×10^{-26} $cm^2 \cdot molecule^{-1} \cdot sr^{-1}$ to 4.2×10^{-26} $cm^2 \cdot molecule^{-1} \cdot sr^{-1}$; for AAO, the frequency upshifts from 1170 cm^{-1} to 1176 cm^{-1}, while the cross section monotonically decreases from 9.1×10^{-26} $cm^2 \cdot molecule^{-1} \cdot sr^{-1}$ to 5.7×10^{-26} $cm^2 \cdot molecule^{-1} \cdot sr^{-1}$.

We utilize a simple binding model to rationalize the Raman spectral dependences on EG hydration. Upon addition of water into the EG acetonitrile solution, the free EG is bound by water and hydrated:

$$EG + nH_2O \rightleftharpoons EG(H_2O)_n$$

Assuming ideal solution behavior, by definition, the apparent association constant is:

$$K = \frac{[EG(H_2O)_n]}{[EG][H_2O]^n} \quad (4)$$

For a water mole fraction of x, the relative fraction of dehydrated EG is $\eta(x) = [EG]/([EG]_{Total})$; then eq 4 is:

$$\eta(x) = \frac{1}{1 + K[H_2O]^n} \quad (5)$$

It is possible to obtain an explicit expression of $[H_2O]$ in terms of x from the densities and molecular weights of water and acetonitrile and assuming ideal solution behavior:

$$[H_2O]/mol \cdot L^{-1} = \frac{1.06 \times 10^3 x}{55.4 - 36.2x} \quad (6)$$

The apparent Raman cross section can be treated as a sum of the cross sections of free and bound EG:

$$\sigma(x) = (1 - \eta(x)) \cdot \sigma_{EG(H_2O)_n} + \eta(x) \cdot \sigma_{EG} \quad (7)$$

By combining eqs 4, 5, and 6, eq 7 becomes:

$$\sigma = \sigma_{EG(H_2O)_n} + \frac{\sigma_{EG} - \sigma_{EG(H_2O)_n}}{1 + K\left(\frac{1.06 \times 10^3 x}{55.4 - 36.2x}\right)^n} \quad (8)$$

Fitting the EG data to eq 8 gives $\sigma_{EG} = (6.6 \pm 0.2) \times 10^{-26}$ $cm^2 \cdot molecule^{-1} \cdot sr^{-1}$, $\sigma_{EG(H_2O)_n} = (4.1 \pm 0.2) \times 10^{-26}$ $cm^2 \cdot molecule^{-1} \cdot sr^{-1}$, $n = 1.8 \pm 0.5$, and $K = 0.19 \pm 0.11$ (Figure 8). In the case of AAO, $\sigma_{AAO} = (8.8 \pm 0.3) \times 10^{-26}$ $cm^2 \cdot molecule^{-1} \cdot sr^{-1}$, $\sigma_{AAO(H_2O)_n} = (5.9 \pm 0.4) \times 10^{-26}$ $cm^2 \cdot molecule^{-1} \cdot sr^{-1}$, $n = 2.1 \pm 0.9$, and $K = 0.09 \pm 0.10$ (Figure 8).

This hydration model is highly simplified. This model can only distinguish between hydrated and dehydrated EG in solution. n, representing the phenomenological hydration level of the molecule, is ~1.8 for EG and ~2.1 for AAO, suggesting that the Gdn group binds ~2 water molecules. This is consistent with previous reports on the hydration of the Gdn compounds.[23−27] The formation of Gdn dimers[23−25,50] possibly accounts for this low hydration level.

Different Environments in Peptides. Previously, we found that the ~1170 cm^{-1} Arg bands in the UVRR spectra of two similar alanine based 21 residue peptides, AP ($A_8RA_4RA_4RA_2$)

dx.doi.org/10.1021/jp404030u | J. Phys. Chem. B 2013, 117, 7145−7156

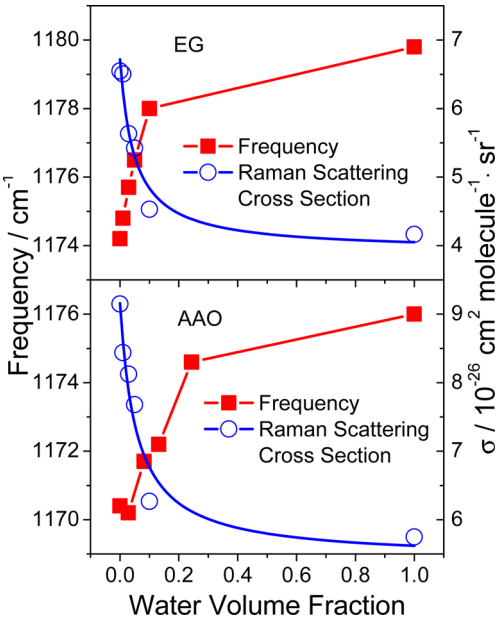

Figure 8. Integrated Raman scattering cross sections and frequencies of the ~1170 cm^{-1} band measured from the 204 nm excited UVRR spectra of EG and AAO in different acetonitrile−water solutions.

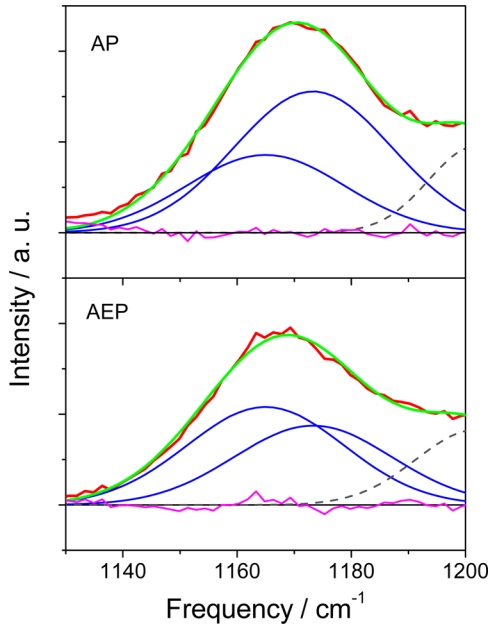

Figure 9. Fitting of the UVRR bands of the Arg side chains in AP and AEP using two Gaussian bands. The dashed bands are tentatively assigned to the backbone $AmIII_3$ bands of turn structures.

and AEP ($A_9RA_3EA_4RA_2$), consist of at least two components ascribed to their different hydration states (see Figure 3 of ref 51). We modeled the hydration dependence of the ~1170 cm^{-1} Arg UVRR band by assuming that the Raman band shape $S(\nu)$ has contributions from two different hydrated forms:

$$S(\nu) = w_{FH}S_{FH}(\nu) + w_{DH}S_{DH}(\nu) \quad (9)$$

where w_{FH} and w_{DH} are the relative fractions ($w_{FH} + w_{DH} = 1$) of the fully hydrated and dehydrated forms, and $S_{FH}(\nu)$ and $S_{DH}(\nu)$ are the Raman spectra of these two forms. The dehydrated form occurs only within the α-helical conformation with a fractional content of ϕ_{DH}:

$$w_{DH} = f_H\phi_{DH} \quad (10)$$

where f_H is the helical fraction. The fully hydrated form occurs in the PPII-like conformations because the Arg side chains should be fully hydrated in these extended conformations. It also appears that some Arg side chains are fully hydrated in the α-helical form. In the α-helical conformation the fully hydrated fraction of the Arg side chain is $\phi_{FH} = 1 - \phi_{DH}$, therefore:

$$w_{FH} = 1 - w_{DH} = f_U + f_H\phi_{FH} = f_U + f_H(1 - \phi_{DH}) \quad (11)$$

where $f_U = 1 - f_H$ is the fraction of PPII-like conformation.

The ~1170 cm^{-1} Arg bands of AP and AEP can be fitted with two Gaussians, as shown in Figure 9, one of which derives from the fully hydrated component with a higher frequency; a second Gaussian with a lower frequency is found to model the dehydrated component. We globally fitted the Arg bands of AP and AEP with two Gaussians of identical bands widths and frequencies. The fitted dehydrated component appears at 1165 cm^{-1} for both AP and AEP peptides, while the hydrated component is found at 1173 cm^{-1}.

We can estimate the fraction of the dehydrated component, ϕ_{DH}, from the ratio:

$$\frac{I_{DH}}{I_{FH}} = \frac{w_{DH}\sigma_{DH}}{w_{FH}\sigma_{FH}} = \frac{f_H\phi_{DH}\sigma_{DH}}{[f_U + f_H(1 - \phi_{DH})]\sigma_{FH}} \quad (12)$$

Rearranging eq 12, we get:

$$\phi_{DH} = \frac{I_{DH}\sigma_{FH}}{f_H(I_{FH}\sigma_{DH} + I_{DH}\sigma_{FH})} \quad (13)$$

where I_{DH} and I_{FH} are the integrated band intensities of the dehydrated and fully hydrated components respectively. $\sigma_{DH} = \int S_{DH}(\nu)\, d\nu$ and $\sigma_{FH} = \int S_{FH}(\nu)\, d\nu$ are the integrated Raman scattering cross sections of the ~1170 cm^{-1} band, which are assumed to be equal to the cross sections of AAO in acetonitrile and in water, respectively. I_{DH} and I_{FH} are obtained by fitting the measured 1170 cm^{-1} UVRR band with two Gaussian bands.

The dehydrated fractions, w_{DH}, are estimated to be 0.27 for AP and 0.45 for AEP. Using our calculated α-helical fraction, f_H, of 0.51 at 4 °C for AEP and AP, we further estimate from eq 13 that, on average, $\phi_{DH} = 0.53$ for the three Arg side chains of AP, while $\phi_{DH} = 0.89$ for the two Arg side chains of AEP.

We can identify four Arg side chain states in AP or AEP: (1) the dehydrated Arg side chain in the PPII-like unfolded state, Arg^U; (2) the hydrated Arg side chain in the PPII-like unfolded state, $Arg(H_2O)^U_{2.1}$; (3) the hydrated Arg side chain in the α-helix folded state, $Arg(H_2O)^F_{2.1}$; and (4) the dehydrated Arg side chain in the α-helix folded state, Arg^F. Scheme 1 shows the thermodynamic cycle between these side chain states. Table 9 gives the fractions of these four Arg side chain states, equilibrium

Scheme 1. Thermodynamic Cycle That Describes the Transition among Four Arg States in the Peptides AP and AEP

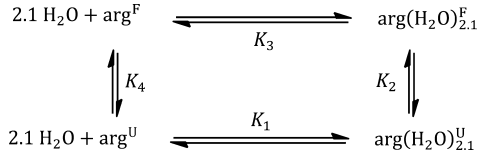

dx.doi.org/10.1021/jp404030u | J. Phys. Chem. B 2013, 117, 7145−7156

constants, and corresponding Gibbs free energies of the transition between these four states.

Table 9. Fractions of Different Arg Hydration States, Equilibrium Constants and Corresponding Gibbs Free Energies in AP and AEP Peptides

peptide	AP	AEP
fraction of Arg^{U} [a]	0.0 ± 0.2	0.0 ± 0.5
fraction of $Arg(H_2O)_{2.1}^{U}$ [a]	0.49 [b]	0.49 [b]
fraction of $Arg(H_2O)_{2.1}^{F}$ [a]	0.24 ± 0.23	0.06 ± 0.5
fraction of Arg^{F} [a]	0.27 ± 0.23	0.45 ± 0.5
$K_1/M^{-2.1}$ [c]	0.09 ± 0.10	0.09 ± 0.10
K_2	0.5 ± 0.5	0.1 ± 1
$K_3/M^{2.1}$ [c]	(5 ± 5) × 10^3	(4 ± 30) × 10^4
K_4	0.004 ± 0.008	0.003 ± 0.03
ΔG_1/kJ·mol^{-1}	6.0 ± 2.7	6.0 ± 2.7
ΔG_2/kJ·mol^{-1}	1.8 ± 2.4	5 ± 22
ΔG_3/kJ·mol^{-1}	−21 ± 2.2	−26 ± 22
ΔG_4/kJ·mol^{-1}	13 ± 4	15 ± 31

[a] These Arg states are defined in Scheme 1. [b] The helical fraction of AP is estimated from ref 3; the AEP helical fraction is identical to AP, see ref 51 for more details. [c] As defined in Scheme 1, K_1 has a unit of $M^{-2.1}$ due to the binding of 2.1 H_2O molecules; K_3 has a unit of $M^{2.1}$ due to the releasing of 2.1 H_2O molecules.

It appears that the Arg side chains in the α-helical conformation are mainly dehydrated. These Arg side chains likely pack against the α-helix backbone where they are shielded from water. This packing also protects the α-helix intrapeptide hydrogen bonds from water, which increases the α-helix stability. This configuration is consistent with García's MD simulations.[52] This packing process releases bound water molecules from the Arg side chains and eliminates the unfavorable interactions between water and Arg side chains. Thus, it is favorable for the peptides to fold into α-helix conformations. The Arg side chains in AEP are less hydrated than those in AP, most likely due to the presence of more α-helix-turn-α-helix conformations[51] that may further shield the Arg side chains from the access of water.

CONCLUSION

We used UVRR spectroscopy and DFT calculations to examine resonance Raman enhancement in Gdn, EG, Arg, and AAO. We examined the calculated ground and first excited state structures and assigned most of the UVRR bands above 1100 cm^{-1}. We have examined the origin of resonance enhancement of the Gdn side chain vibrations. The UVRR scattering cross section and the frequency of the ∼1170 cm^{-1} Arg band in peptides and proteins provide monitors for the local environment of the Gdn group. To rationalize the cross section dependence on hydration, a simple hydration model was applied to EG and AAO. By applying this model to two polyAla peptides, AP and AEP, both containing Arg residues, we were able to identify different hydration states for different conformations. It was found that the AEP Arg side chain in the α-helical conformation is more dehydrated than the AP Arg side chain in its α-helical conformation.

AUTHOR INFORMATION

Notes

The authors declare no competing financial interest.

ACKNOWLEDGMENTS

We thank Dr. Bhavya Sharma for helpful discussions. This work was supported by NIH Grant 5RO1 EB002053 and NIH 1RO1 EB009089, and in part by the University of Pittsburgh Center for Simulation and Modeling through the supercomputing resources provided.

REFERENCES

(1) Asher, S. A. *Anal. Chem.* **1993**, *65*, A201.
(2) Asher, S. A. *Anal. Chem.* **1993**, *65*, A59.
(3) Lednev, I. K.; Karnoup, A. S.; Sparrow, M. C.; Asher, S. A. *J. Am. Chem. Soc.* **1999**, *121*, 8074.
(4) Lednev, I. K.; Karnoup, A. S.; Sparrow, M. C.; Asher, S. A. *J. Am. Chem. Soc.* **1999**, *121*, 4076.
(5) Asher, S. A.; Ianoul, A.; Mix, G.; Boyden, M. N.; Karnoup, A.; Diem, M.; Schweitzer-Stenner, R. *J. Am. Chem. Soc.* **2001**, *123*, 11775.
(6) Asher, S. A.; Mikhonin, A. V.; Bykov, S. *J. Am. Chem. Soc.* **2004**, *126*, 8433.
(7) Mikhonin, A. V.; Asher, S. A. *J. Am. Chem. Soc.* **2006**, *128*, 13789.
(8) Mikhonin, A. V.; Bykov, S. V.; Myshakina, N. S.; Asher, S. A. *J. Phys. Chem. B* **2006**, *110*, 1928.
(9) Oladepo, S. A.; Xiong, K.; Hong, Z.; Asher, S. A. *J. Phys. Chem. Lett.* **2011**, *2*, 334.
(10) Oladepo, S. A.; Xiong, K.; Hong, Z.; Asher, S. A.; Handen, J.; Lednev, I. K. *Chem. Rev.* **2012**, *112*, 2604.
(11) Asher, S. A.; Ludwig, M.; Johnson, C. R. *J. Am. Chem. Soc.* **1986**, *108*, 3186.
(12) Fodor, S. P. A.; Copeland, R. A.; Grygon, C. A.; Spiro, T. G. *J. Am. Chem. Soc.* **1989**, *111*, 5509.
(13) Chi, Z. H.; Asher, S. A. *J. Phys. Chem. B* **1998**, *102*, 9595.
(14) Sweeney, J. A.; Asher, S. A. *J. Phys. Chem.* **1990**, *94*, 4784.
(15) Miura, T.; Takeuchi, H.; Harada, I. *J. Raman Spectrosc.* **1989**, *20*, 667.
(16) Miura, T.; Takeuchi, H.; Harada, I. *Biochemistry* **1991**, *30*, 6074.
(17) Takeuchi, H. *Biochemistry* **1997**, *36*, 10993.
(18) Takeuchi, H. *Biopolymers* **2003**, *72*, 305.
(19) Hildebrandt, P. G.; Copeland, R. A.; Spiro, T. G.; Otlewski, J.; Laskowski, M.; Prendergast, F. G. *Biochemistry* **1988**, *27*, 5426.
(20) Asher, S. A.; Murtaugh, J. L. *Appl. Spectrosc.* **1988**, 42.
(21) Sension, R. J.; Hudson, B.; Callis, P. R. *J. Phys. Chem.* **1990**, *94*, 4015.
(22) Wolfenden, R.; Andersson, L.; Cullis, P. M.; Southgate, C. C. B. *Biochemistry* **1981**, *20*, 849.
(23) Mason, P. E.; Dempsey, C. E.; Neilson, G. W.; Brady, J. W. *J. Phys. Chem. B* **2005**, *109*, 24185.
(24) Mason, P. E.; Neilson, G. W.; Dempsey, C. E.; Barnes, A. C.; Cruickshank, J. M. *Proc. Natl. Acad. Sci. U.S.A.* **2003**, *100*, 4557.
(25) Mason, P. E.; Neilson, G. W.; Kline, S. R.; Dempsey, C. E.; Brady, J. W. *J. Phys. Chem. B* **2006**, *110*, 13477.
(26) Hunger, J.; Niedermayer, S.; Buchner, R.; Hefter, G. *J. Phys. Chem. B* **2010**, *114*, 13617.
(27) McQuinn, K.; McIndoe, J. S.; Hof, F. *Chem.—Eur. J.* **2008**, *14*, 6483.
(28) García, A. E.; Stiller, L. *J. Comput. Chem.* **1993**, *14*, 1396.
(29) White, S. H.; Wimley, W. C. *Annu. Rev. Biophys. Biomol. Struct.* **1999**, *28*, 319.
(30) Sharma, B.; Asher, S. A. *J. Phys. Chem. B* **2011**, *115*, 5659.
(31) Bykov, S.; Lednev, I.; Ianoul, A.; Mikhonin, A.; Munro, C.; Asher, S. A. *Appl. Spectrosc.* **2005**, *59*, 1541.
(32) Dudik, J. M.; Johnson, C. R.; Asher, S. A. *J. Chem. Phys.* **1985**, *82*, 1732.
(33) Frisch, M. J.; Trucks, G. W.; Schlegel, H. B.; Scuseria, G. E.; Robb, M. A.; Cheeseman, J. R.; Scalmani, G.; Barone, V.; Mennucci, B.; Petersson, G. A.; Nakatsuji, H.; Caricato, M.; Li, X.; Hratchian, H. P.; Izmaylov, A. F.; Bloino, J.; Zheng, G.; Sonnenberg, J. L.; Hada, M.; Ehara, M.; Toyota, K.; Fukuda, R.; Hasegawa, J.; Ishida, M.; Nakajima, T.; Honda, Y.; Kitao, O.; Nakai, H.; Vreven, T.; Montgomery, J. A., Jr.; Peralta, J. E.; Ogliaro, F.; Bearpark, M.; Heyd, J. J.; Brothers, E.; Kudin,

K. N.; Staroverov, V. N.; Keith, T.; Kobayashi, R.; Normand, J.; Raghavachari, K.; Rendell, A.; Burant, J. C.; Iyengar, S. S.; Tomasi, J.; Cossi, M.; Rega, N.; Millam, J. M.; Klene, M.; Knox, J. E.; Cross, J. B.; Bakken, V.; Adamo, C.; Jaramillo, J.; Gomperts, R.; Stratmann, R. E.; Yazyev, O.; Austin, A. J.; Cammi, R.; Pomelli, C.; Ochterski, J. W.; Martin, R. L.; Morokuma, K.; Zakrzewski, V. G.; Voth, G. A.; Salvador, P.; Dannenberg, J. J.; Dapprich, S.; Daniels, A. D.; Farkas, O.; Foresman, J. B.; Ortiz, J. V.; Cioslowski, J.; Fox, D. J. *Gaussian 09*; Gaussian, Inc.: Wallingford, CT, 2010.

(34) Groner, P. *Normal Coordinate Analysis*; John Wiley & Sons, Ltd.: New York, 2006.

(35) McIntosh, D. *Theor. Chem. Acc.* **2009**, *125*, 177.

(36) Pulay, P.; Fogarasi, G.; Pang, F.; Boggs, J. E. *J. Am. Chem. Soc.* **1979**, *101*, 2550.

(37) Tang, W.; Sanville, E.; Henkelman, G. *J. Phys.: Condens. Matter* **2009**, *21*, 084204.

(38) Sanville, E.; Kenny, S. D.; Smith, R.; Henkelman, G. *J. Comput. Chem.* **2007**, *28*, 899.

(39) Henkelman, G.; Arnaldsson, A.; Jónsson, H. *Comput. Mater. Sci.* **2006**, *36*, 354.

(40) Magalhães, A. L.; Gomes, J. A. N. F. *Int. J. Quantum Chem.* **1997**, *61*, 725.

(41) Gobbi, A.; Frenking, G. *J. Am. Chem. Soc.* **1993**, *115*, 2362.

(42) Mak, M. L.; Salpietro, S. J.; Enriz, R. D.; Csizmadia, I. G. *Can. J. Chem.* **2000**, *78*, 626.

(43) Walsh, A. D. *J. Chem. Soc.* **1953**, 2301.

(44) Heller, E. J. *J. Chem. Phys.* **1975**, *62*, 1544.

(45) Heller, E. J.; Sundberg, R.; Tannor, D. *J. Phys. Chem.* **1982**, *86*, 1822.

(46) Tannor, D. J.; Heller, E. J. *J. Chem. Phys.* **1982**, *77*, 202.

(47) Lee, S.-Y.; Heller, E. J. *J. Chem. Phys.* **1979**, *71*, 4777.

(48) Braiman, M. S.; Briercheck, D. M.; Kriger, K. M. *J. Phys. Chem. B* **1999**, *103*, 4744.

(49) Vanderkooi, J. M.; Dashnau, J. L.; Zelent, B. *Biochim. Biophys. Acta* **2005**, *1749*, 214.

(50) No, K. T.; Nam, K.-Y.; Scheraga, H. A. *J. Am. Chem. Soc.* **1997**, *119*, 12917.

(51) Hong, Z.; Ahmed, Z.; Asher, S. A. *J. Phys. Chem. B* **2011**, *115*, 4234.

(52) García, A. E.; Sanbonmatsu, K. Y. *Proc. Natl. Acad. Sci. U.S.A.* **2002**, *99*, 2782.